Pacific Northwest
NATIONAL LABORATORY

PNNL-35822

Nanoscale Consequences of Irradiation Investigated by RAD-AFM

March 2024

Shawn L Riechers
Alan L Schemer-Kohrn
Mychailo B Toloczko
Danny J Edwards

U.S. DEPARTMENT OF ENERGY

Prepared for the U.S. Department of Energy
under Contract DE-AC05-76RL01830

DISCLAIMER

PACIFIC NORTHWEST NATIONAL LABORATORY
operated by
BATTELLE
for the
UNITED STATES DEPARTMENT OF ENERGY
under Contract DE-AC05-76RL01830

Printed in the United States of America

Available to DOE and DOE contractors from
the Office of Scientific and Technical Information,
P.O. Box 62, Oak Ridge, TN 37831-0062
www.osti.gov
ph: (865) 576-8401
fox: (865) 576-5728
email: reports@osti.gov

Available to the public from the National Technical Information Service
5301 Shawnee Rd., Alexandria, VA 22312
ph: (800) 553-NTIS (6847)
or (703) 605-6000
email: info@ntis.gov
Online ordering: http://www.ntis.gov

PNNL-35822

Nanoscale Consequences of Irradiation Investigated by RAD-AFM

March 2024

Shawn L Riechers
Alan L Schemer-Kohrn
Mychailo B Toloczko
Danny J Edwards

Prepared for
the U.S. Department of Energy
under Contract DE-AC05-76RL01830

Pacific Northwest National Laboratory
Richland, Washington 99354

Summary

This report details the methods developed and observational findings of this Laboratory Directed Research and Development project. The objective of this project was to assess the ability of Atomic Force Microscopy (AFM) analysis to detect changes that are uniquely observable by this method induced by different irradiation protocols. More specifically to investigate the ability to detect microstructural and micromechanical changes induced by ion irradiation, neutron irradiation, and sequential neutron and ion irradiation, ultimately to determine if ion irradiation can produce material property changes that faithfully replicate neutron irradiation. AFM is a powerful tool for providing material property characterization at lateral resolutions sufficient for probing ion irradiated cross sections (Kautz et al. 2023; Riechers et al. 2020; Kaspar et al. 2019), where the penetration depth of the ions is typically on the order of hundreds of nanometers.

A previous Nuclear Energy Enabling Technologies Program task carried out at PNNL (2018) provides an excellent test bed for the development of an AFM approach to measure material properties resulting from a combination of ion and neutron irradiation. This effort utilized TEM and APT analysis on a matrix of HT-9 samples to compare pure ion irradiation, neutron + ion irradiation, and pure neutron irradiation to a total dose of 112 and 250 DPA at temperatures ranging from 375 to 460°C. HT-9 is a class of tempered martensitic steel alloys which are being considered as candidate materials for advanced reactors that show excellent void swelling resistance to doses over 200 Displacements per atom (DPA). Neutron irradiation of such materials considered for nuclear applications is required to test their performance. However, neutron irradiation has several disadvantages from an experimental standpoint: it is 1) expensive, 2) time consuming, and 3) results in radioactive materials. Ion irradiation is an improvement on all three counts and is often utilized to speed the research and development process by utilizing a shift in irradiation temperature to achieve more similar effects. However, the resulting microstructure of ion irradiated materials is often unlike their neutron irradiated counterparts. By carrying out ion irradiation on previously neutron irradiated materials it was hypothesized ion irradiation could be used to increase the accumulated irradiation dose of the “preconditioned” microstructure of the neutron irradiated samples. While this approach did not fully provide the intended effect of reproducing all neutron-only microstructures a critical piece of information that was lacking was the ability to measure the local mechanical and physical properties at the ion irradiated regions. Three legacy samples from this effort were chosen for this current work that had the same total dose of 112 DPA irradiated at 412°C.

AFM analysis was carried out with a unique rad capable multimodal AFM located in the RPL microscopy suite. It is capable of measuring dozens of physical properties including topography, hardness, thermal conductivity, and piezo response with a lateral resolution of 1-10s of nm depending on the mode. This capability has been developed for use with radioactive materials and has been demonstrated with both ion and neutron irradiated materials for the Tritium Modernization Program.(Riechers et al. 2020; Riechers et al. 2018; Riechers and Johnson 2018)

The chosen HT-9 samples were cross sectioned and prepared specifically for AFM tapping mode and hardness mapping. Co-located SEM-EDS was used to confirm the presence of silver and tungsten that were used to cap the ion irradiated side and prevent carbon contamination. AFM hardness was optimized for HT-9 and calibrated using reference materials. The measured AFM hardness was uniform across the entire cross section from the ion irradiated face through the bulk with the exception of an increase at the unpolished back face. Comparisons of the bulk

pristine, 37 DPA and 112 DPA neutron irradiated HT-9 revealed an overall increase in hardness as expected due to radiation hardening. High resolution imaging at the ion irradiated surface showed a mild increase in hardness at 112 DPA, and no apparent change at the 75 DPA ion, 37 DPA neutron irradiated surface. A lateral resolution of ~150 nm during hardness mapping was achieved.

Acknowledgments

The research described in this report was conducted under the Laboratory Directed Research and Development Program at Pacific Northwest National Laboratory, a multiprogram national laboratory operated by Battelle for the U.S. Department of Energy. The AFM analysis was conducted on the RAD-AFM a Nuclear Science User Facility (NSUF) instrument which is also part of the Radiological Microscopy Suite within the Radiochemical Processing Laboratory (RPL) located at Pacific Northwest National Laboratory.

Acronyms and Abbreviations

AFM – Atomic Force Microscopy

BSE – Backscattered Electron (imaging)

DPA- Displacements per atom

EBSD – Electron backscattered diffraction

EDS – Energy Dispersive X-ray Spectroscopy

FFM – Fast Force Mapping

NSUF– Nuclear Science User Facility

PNNL – Pacific Northwest National Laboratory

RPL – Radiochemical Processing Laboratory

SEM – Scanning Electron Microscopy

STEM – Scanning Transmission Electron Microscopy

SRM – Standard Reference Materials

SEM – Scanning Electron Microscopy

TEM – Transmission Electron Microscopy

Contents

Figures

Tables

1.0 Overview

To assess the feasibility of measuring material property changes induced by ion irradiation one pristine and three legacy HT-9 samples were sectioned and polished. The polish protocol was first optimized using a pristine unirradiated HT-9 sample before polishing the ion irradiated samples as the spot size was small and repeated polishing could remove the ion irradiated region entirely. Atomic force microscopy (AFM) tapping mode was used to assess the surface quality after each polish. AFM based hardness mapping was optimized for new diamond tips specifically for use with the HT-9 samples to compensate for differences in grain size, precipitates, and heterogeneity of hardness relative to past samples. In addition, a hardness calibration protocol was developed using NIST copper, nickel, and steel reference materials. Co-located SEM-EDS and AFM analysis was used to verify the ion irradiated edge using the silver/tungsten coating as a fiducial mark. Once benchmarked, the hardness across the ion irradiated cross section, a comparison of bulk hardness according to neutron irradiation, and the hardness of the ion irradiated surface edge was measured.

1.1 Materials

The legacy HT-9 samples used are composed of 11.9 Cr, 0.2 C, 0.23 Si, 0.50 Mn, 0.50 W, 0.34 V, 1.02 Mo, and 0.58 Ni by weight percent. The ion irradiation dose (denoted as (i)) and the neutron dose (denoted as (n)) are shown in Table 1. The three irradiated samples were chosen as a total dose of 112 DPA was consistent for all three samples allowing for a fair comparison of neutron and ion irradiation effects. Specimens were irradiated by neutrons at 412 °C to 37 and 112 DPA at the Fast Flux Test Facility-Materials Open Test Assembly (FFTF-MOTA). Prior to ion irradiation samples were then coated with 7.1 nm silver followed by 203 nm tungsten using magnetic sputtering based physical vapor deposition to prevent carbon-based contamination. Ion irradiation was carried out at the Texas A&M University Ion Beam Lab using Fe ions with 4 MeV at 412°C. TEM cross sectional analysis performed previously of the 75 DPA (i) + 37 DPA (n) reveals a slight change at the surface, whereas 213 DPA (i) + 37 DPA (n) reveals the presence of void swelling up to a depth of ~1 µm, Figure 1. Due to the smaller scope of this study, sample preparation and AFM analysis could not be performed on the 213 DPA (i) + 37 DPA (n) sample.

Table 1. HT-9 specimens from legacy materials library stored at PNNL.

	ID	Ion DPA	Neutron DPA	Temp. (°C)
Pristine		0	0	0
Ion irradiated	HL10	112	0	412
Neutron irradiated	RT02-IR	0	112	412
Ion/Neutron irradiated	HL02-IR	75	37	412

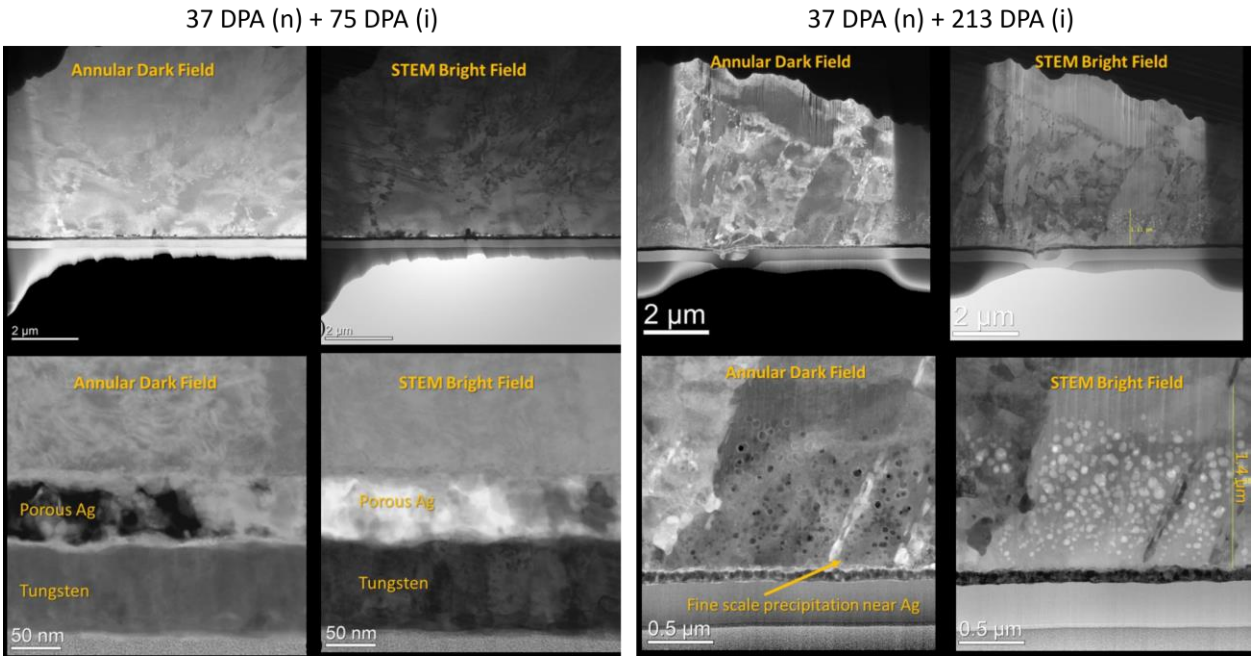

Figure 1. TEM analysis of the 112 DPA ion irradiated sample cross section revealing the silver/tungsten coating. Fiducial marks and the HT-9 edge are highlighted in the SEM and Co-located AFM.

1.2 Sample Preparation

Samples were cut through the ion irradiated region with an offset to ensure the final cross-sectional surface represented the center of the ion irradiated region. This process in relation to the coating, ion irradiation, and sample mounting is shown in Figure 2. Samples were then affixed to the bottom of a 1" metallographic 2-part mounting cup using a thin film of superglue to ensure the samples didn't not move/float in the epoxy resin used to cast the mount. Once cured it was removed from the mounting cup and fixtured into a Buehler MiniMet sample cage (designed for a 1" mount). Grinding steps were performed using water and 9 total passes, 90 seconds each progressing from 320, 400, 600, 800, and 1200 grit. To accommodate a specialized AFM sample holder for future work, the samples were cut to reduce the final height to <2.5 mm using a mount vice and a Buehler Isomet low speed saw.

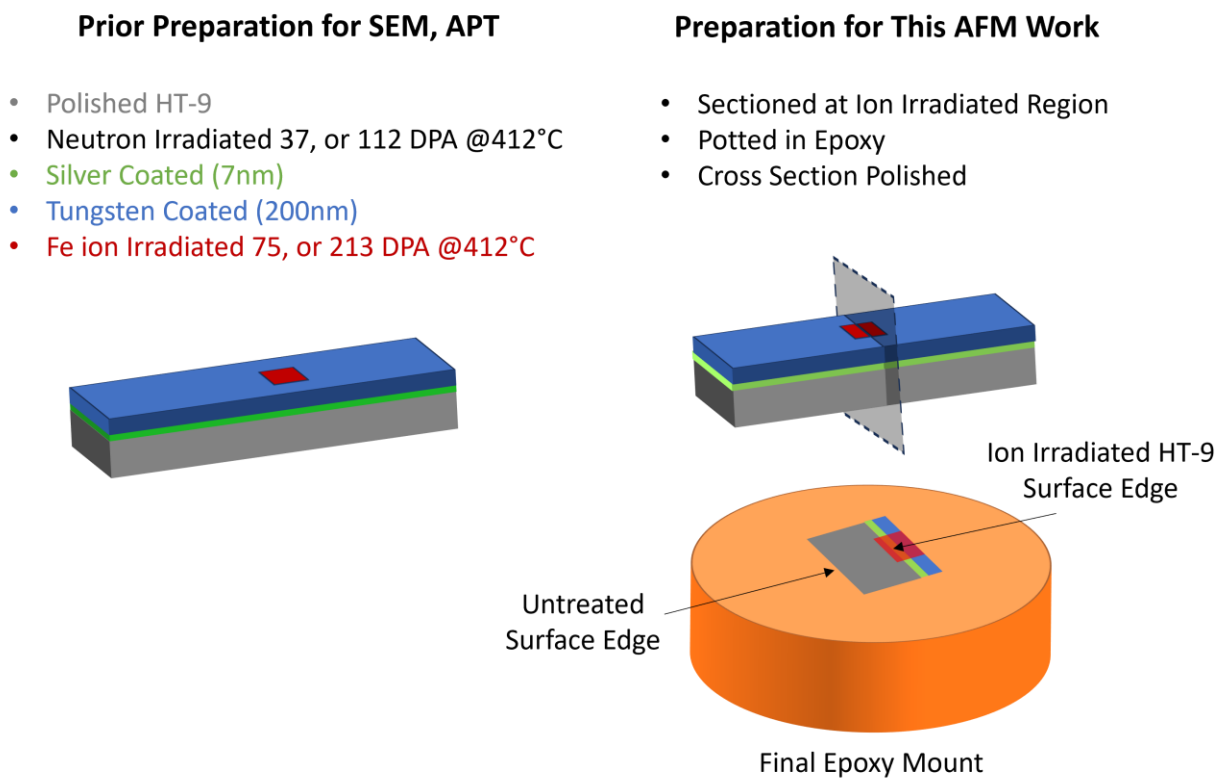

Figure 2. Outline of sample preparation workflow for past and current work. Coating thickness is greatly exaggerated for clarity.

The slice was then taped to a sacrificial “shim” and fixtured into the MiniMet sample cage. Final polishing steps were then performed, 30 minutes each using 9, 6, 3, and 1µm polycrystalline diamond compound. After fine polishing was performed using the MiniMet, the sample slice was then taped to a 1 lb weight, placed into a vibratory polisher using 0.02 micron colloidal silica suspension and run overnight. Once the sample is removed from the vibratory polisher, it was immediately rinsed with DI water, mechanically cleaned with a wet cotton ball, rinsed again and dried with canned air. Ultrasonic cleaning was then performed for 3 minutes each using soapy water, DI water, and ethanol. Initial analysis revealed a relatively poor finish for AFM which is highly sensitive to surface coatings, remaining polishing compounds, and particles. An additional 0.5% acetic acid ultrasonic cleaning step was added after the DI water, which greatly improved surface quality as shown in Figure 3.

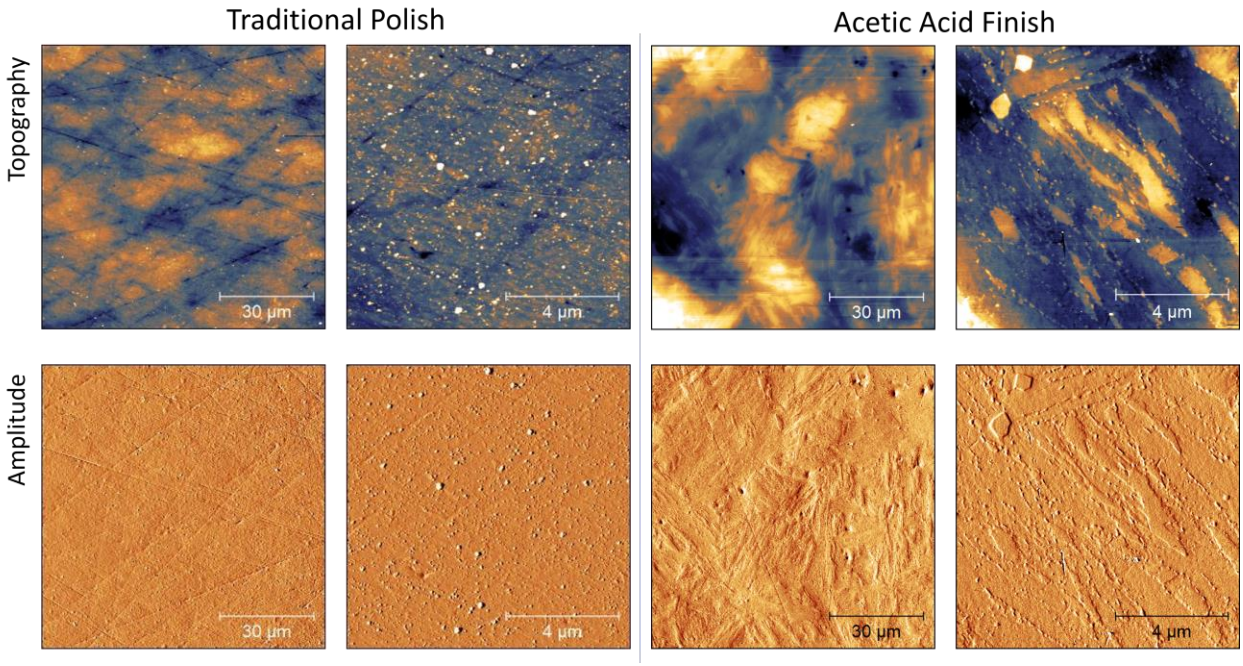

Figure 3. Comparison of the pristine HT-9 surface morphology given by AFM tapping mode analysis after traditional polishing methods and a traditional polishing followed by acetic acid treatment.

2.0 Results and Discussion

2.1 Surface Morphology

Surface morphology, measured by tapping mode AFM, varied between the three irradiated samples as shown in Figure 4. As the regions shown are far from the ion irradiated surface edge, these regions correlate to unirradiated, 37 DPA (n), and 112 DPA (n) irradiated HT-9. Smaller, easily distinguishable grains were observed on the unirradiated polished surface, while larger less defined grains with precipitates decorating grain boundaries are apparent on the 37 DPA (n), and few well defined features are distinguishable on the 112 DPA (n). The observed variation in morphology is likely due in part to different levels of oxidation as time between polishing and imaging was not held constant.

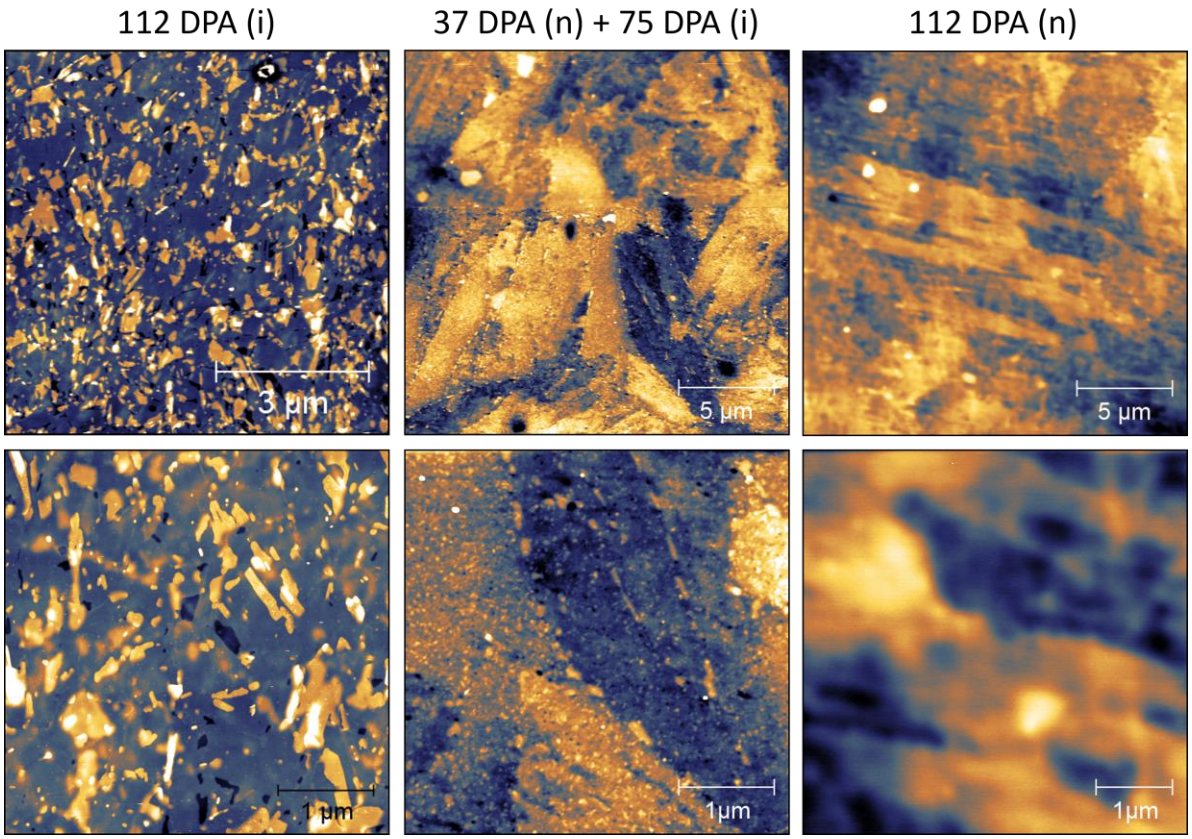

Figure 4. AFM topography showcasing the bulk surface morphology of the ion, neutron and ion, and neutron only irradiated samples.

2.2 AFM Hardness Mapping

AFM hardness mapping, the focus of this work, is a technique which is highly sensitive to the parameters under which the image is acquired. This imaging mode utilizes a diamond tip to press into the surface of the sample in a manner similar to micro or nanoindentation, but with a much smaller tip, penetration depth, and therefore higher resolution. Thousands of indents are

acquired in a short timeframe, for instance in the images shown in Figure 5, 256 by 256 indents are acquired in 9 minutes, or 121 indents per second. The lateral hardness resolution is thus unparalleled, however the interpretation of the resulting hardness values is not straight forward and a great deal of care should be taken to ensure the validity of the resulting hardness values. Parameters such as the indent spacing (pixels/image area), indentation speed, curve fitting algorithm, and indentation setpoint force will impact the hardness values given and their impact will depend on the material being interrogated. Thus, a great deal of work was undertaken, as shown in the following sections, to validate the hardness values given. For example, for the HT-9 samples a setpoint below 50 µN resulted in low contrast and tip artifacts across the surface such as streaking, see Figure 5. In addition, the hardness values given by the software decrease as the setpoint force is increased.

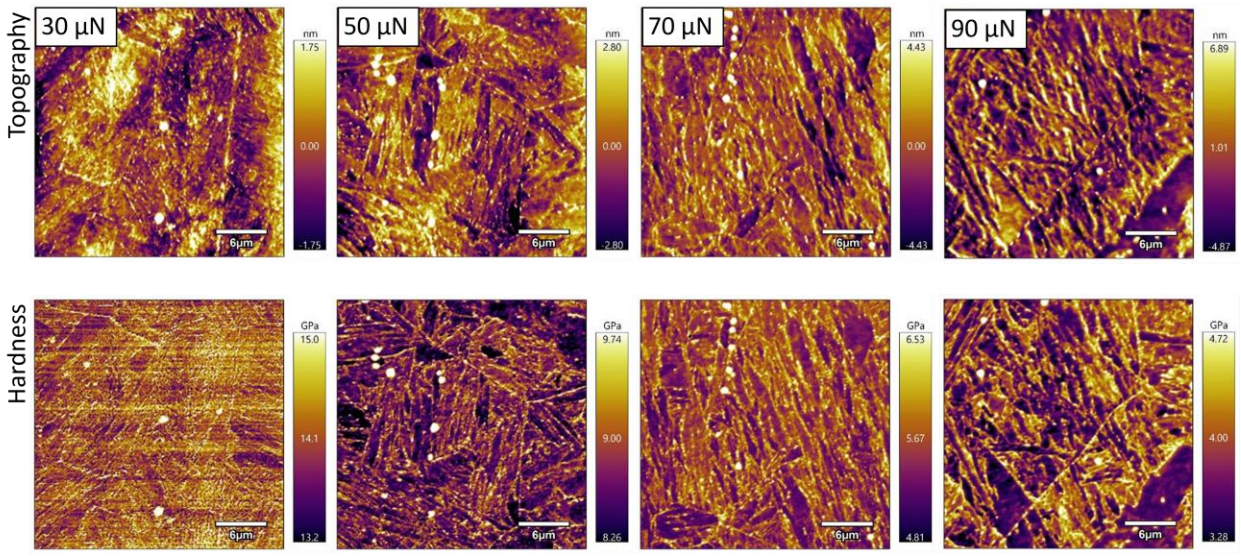

Figure 5. Resulting AFM hardness mapping contrast obtained from applied indentation setpoints of 30, 50, 70, and 90 µN. Hardness values are the given (uncalibrated) AFM values calculated by a Hertz fitting algorithm.

One concern with this method due to the relatively low forces and small tip contact area, was whether the indentations themselves were truly measuring a hardness value resulting from plastic deformation. AFM tapping mode imaging was employed after hardness imaging with an indentation separation of 118 nm, setpoint of 70 µN and resulting penetration depth of ~115 nm. As shown in Figure 6 the individual indents are clearly visible, indicating plastic deformation has occurred. The resulting hardness image is smaller than the indented area due to the software automatically overshooting and removing noisy data at the edges. This discrepancy appears at the top of the image as these were acquired 90 degrees from one another and the hardness image was cropped at the bottom to show only the relevant co-located regions.

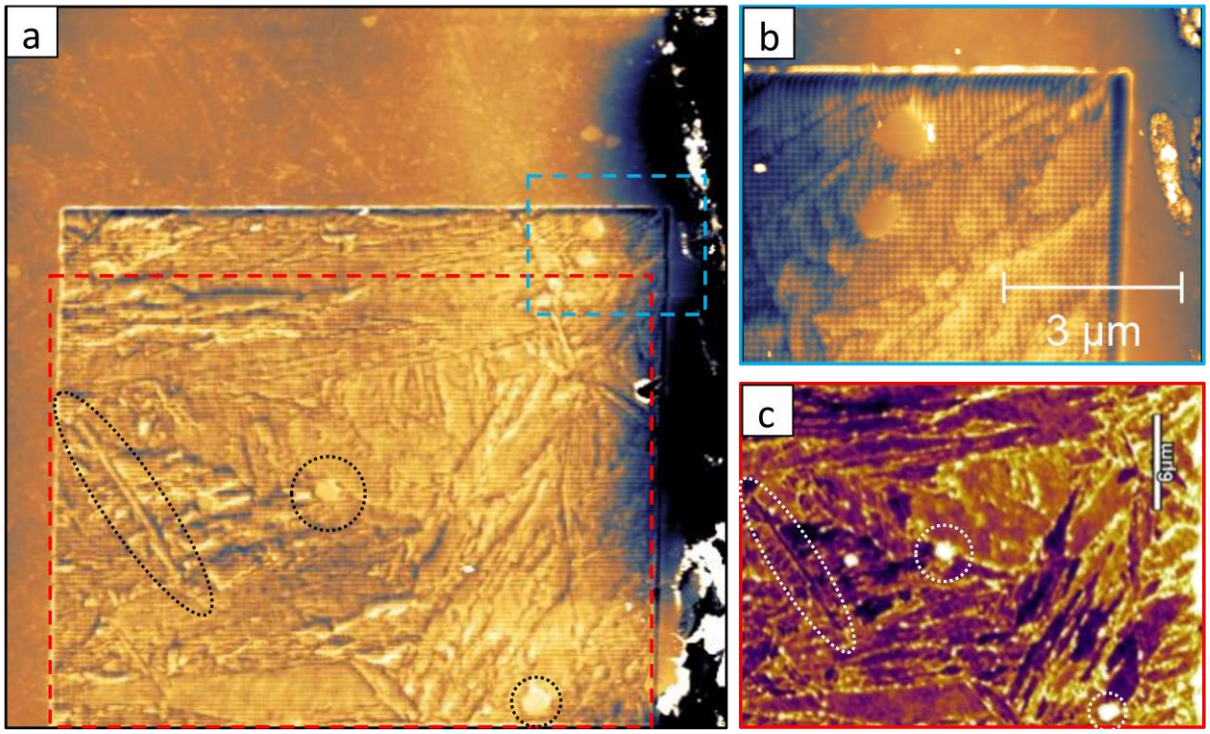

Figure 6. Resulting surface structure alteration after hardness mapping of the 112 DPA (i) sample with a setpoint of 70 µN is revealed by AFM tapping mode (a). Individual indents are clearly resolved at higher resolution in the region indicated by the blue outline (b). The resulting hardness map captured in the region marked by the red outline correlates with the surface features outlined in black and white (c).

To provide a baseline bulk hardness gradient hardness maps were taken along the entire cross section to determine whether ion irradiation had an impact on the observed hardness on a quasi-bulk scale. The hardness map images shown in Figure 7 (a, b) span the entire cross section starting with #1 at the unirradiated and un-polished surface edge to #8, the polished and ion irradiated surface edge. After imaging the location of each hardness map can be identified by a slight change in the optical contrast providing a map for each image as shown in Figure 7 (c). The images were acquired 90 degrees from the optical image, thus the outermost unirradiated edge is the bottom of #1, while the ion irradiated edge is the top of #8. At the unirradiated edge an increase in the topography and corresponding increase in hardness is observed, while no obvious change in hardness is observed at this scale for the ion irradiated region and is also reflected in the average hardness values for each image given in Figure 7 (c).

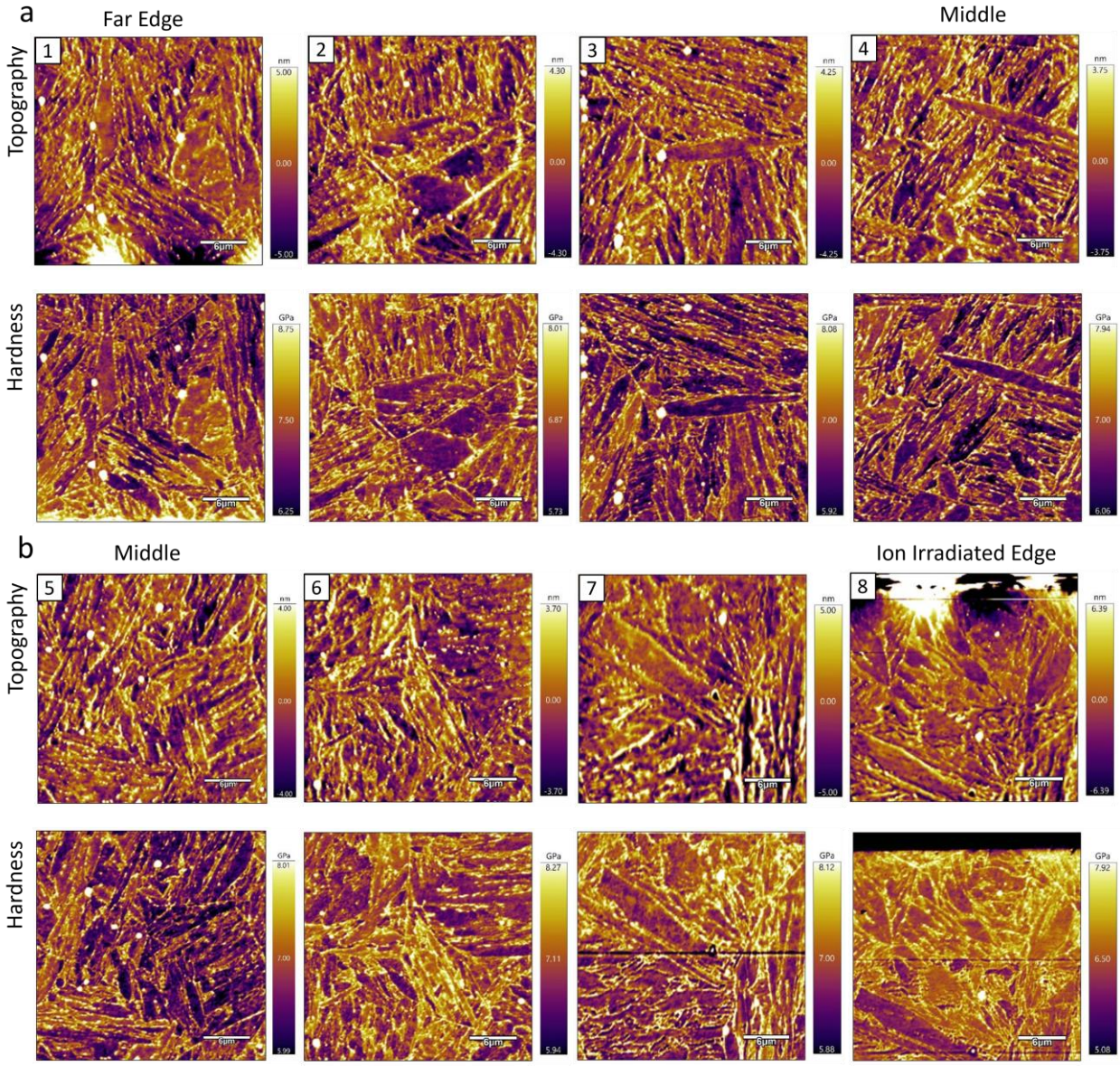
a
Far Edge
Middle
Topography
Hardness
1
2
3
4
b
Middle
Ion Irradiated Edge
5
6
7
8

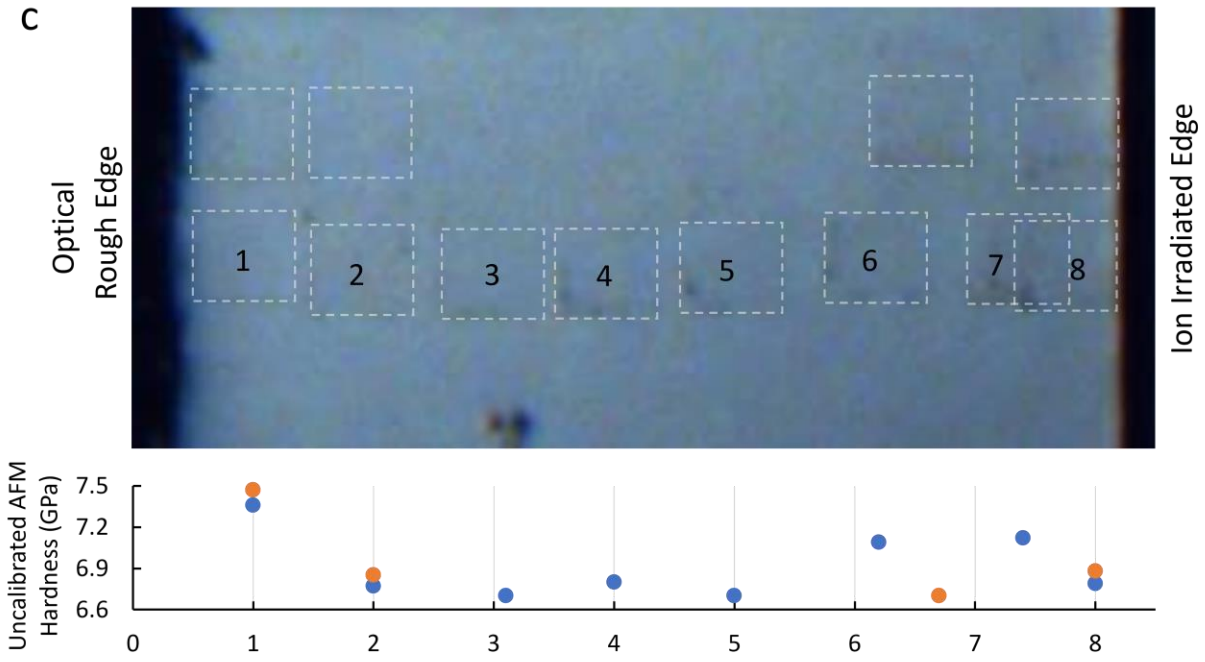

Figure 7. AFM hardness mapping carried out across the entire cross section of the 112 DPA ion irradiated sample from the far edge (a) to the ion irradiated edge (b). Images are rotated 90 degrees counterclockwise. The location of the corresponding hardness mapping regions 1-8 in (a, b) are shown in (c) with the resulting average AFM hardness value (uncalibrated) for each image given in the graph below (additional images corresponding to orange points not shown).

2.3 AFM Hardness Mapping Calibration

Calibration of the AFM hardness maps begins by first determining the optimal imaging conditions for reproducible results. As demonstrated with the indentation setpoint in Figure 5 changing key imaging parameters will alter the image quality, resolution, and given hardness values. Optimization of the indent spacing (pixels/image area), indentation speed, curve fitting algorithm, and indentation setpoint force were first optimized using the 112 (i) sample and three NIST reference materials copper, nickel, and steel providing a range of hardness values. An image size of 30 µm with 256 by 256 pixels, resulting in an indentation separation of 118 nm, an imaging speed of 3 Hz, and a Hertz cone fitting function were determined to provide the most reproducible results while also providing high resolution on each of the reference materials. Using these optimized parameters, the resulting average hardness value given as a result of the indentation setpoint is shown in Figure 8 (a). As the setpoint is increased the given hardness value decreases until a point at which more consistent values are reached. The higher value given for lower forces is likely a convolution of many factors that ultimately are due to differences in surface vs bulk properties and their effect on the measurement, such as local surface roughness and oxide layers. These surface affects are dependent on the material and diminish as the higher setpoint forces are used and more subsurface material is probed. Thus, higher setpoint values provide a better calibration. However, there is a tradeoff. As higher

forces are used the AFM tip penetrates deeper into the material and the lateral resolution, which is the primary advantage of this technique, will suffer due to the greater degree of material that is displaced. Therefore, a setpoint close to the point at which the reported hardness no longer changes for the three reference materials, 90 µN, was chosen and the resulting AFM to Vickers reference curve was obtained as shown in Figure 8 (b).

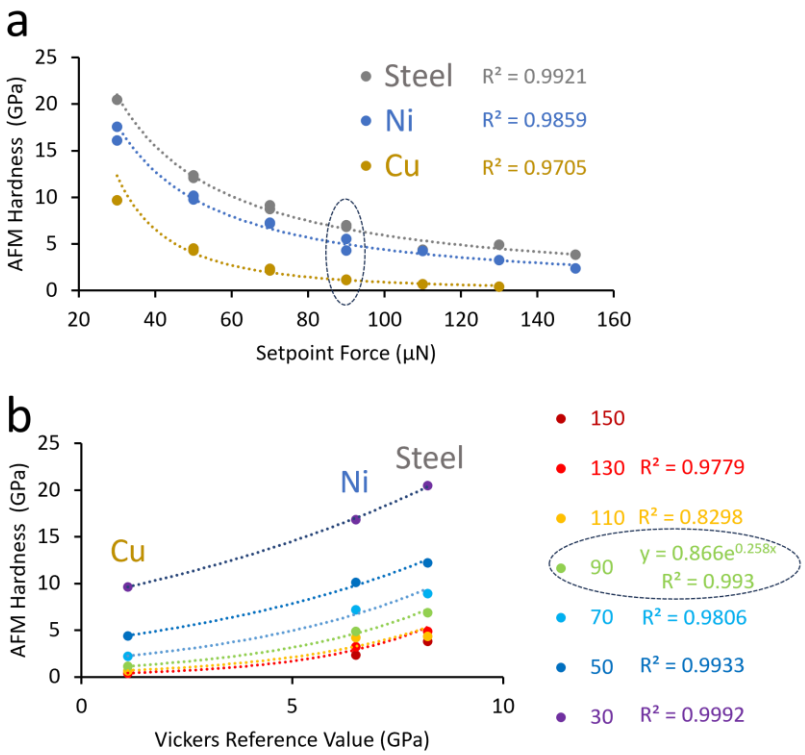

Figure 8. Variation in average AFM hardness values as a function of indentation setpoint force for steel, nickel, and copper NIST reference materials (a). Resulting calibration curves given for each setpoint force (b). The selected setpoint force of 90 µN is highlighted in (a), and (b).

2.4 Neutron Irradiation Induced Hardening

Utilizing the optimized AFM hardness mapping parameters and reference calibration curve the impact of neutron irradiation could be measured. The average of four hardness maps each consisting of more than 65,000 indents was used to provide a comparison bulk value. While AFM hardness mapping provides the local hardness variation across grains, grain boundaries, and precipitates a comparison to bulk Vickers hardness values was estimated by threshold masking to remove harder precipitate values. Representative images of the 0, 37 and 112 DPA (n) samples are shown in Figure 9. The AFM hardness measured for the unirradiated sample was calculated to corresponded to a Vickers hardness value of 5.0 GPa, Table 2. This is 80% higher than that measured by microhardness analysis carried out previously. Radiation hardening was measured as an increase of 4% and 10% for the 37 and 112 DPA (n) respectively by AFM while microhardness analysis reported an increase of 18% and 17%. The values measured by these two techniques are remarkably similar considering the differences in indentation geometry, applied force, and penetration depth. In addition, the microhardness was measured through the ion / neutron irradiated surface into the neutron only region, whereas the

AFM hardness mapping was conducted on freshly polished cross sections consisting only of neutron irradiated HT-9.

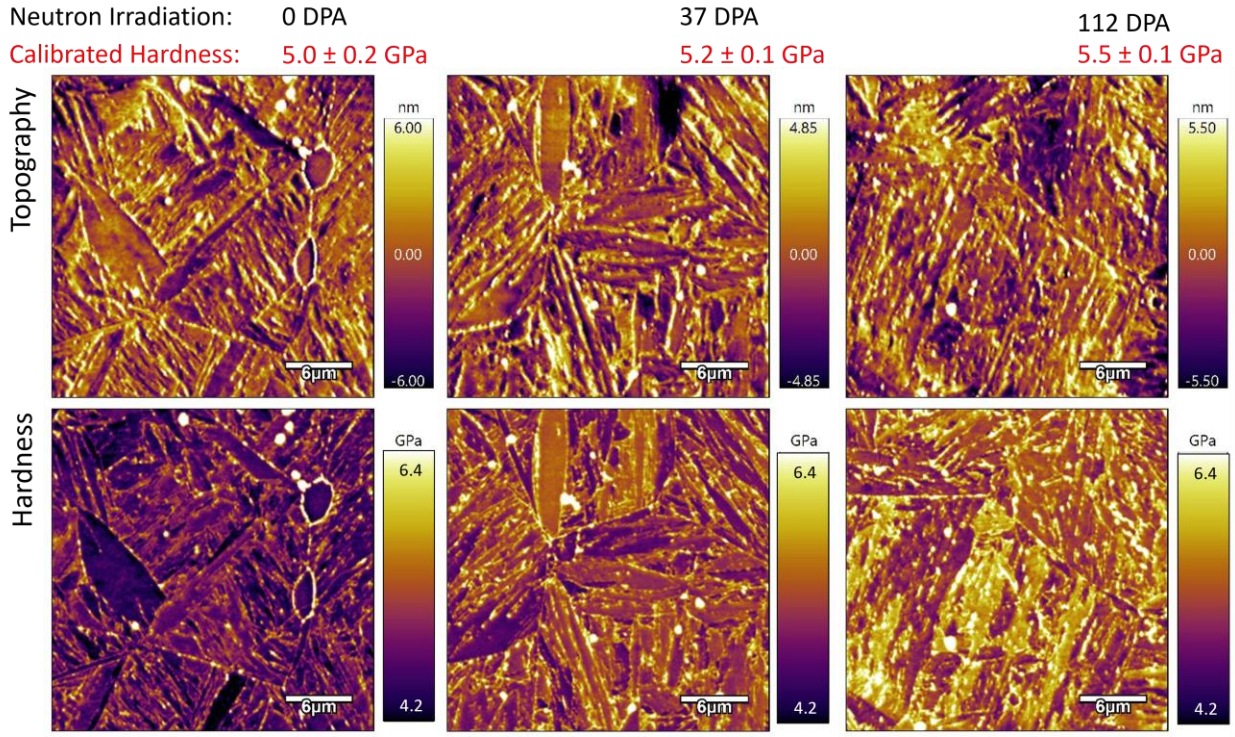

Figure 9. Calibrated AFM hardness mapping of the three samples according to neutron irradiation dose.

Table 2. Neutron Irradiated HT-9 microhardness and calibrated AFM hardness.

(n) DPA	Vickers @ 2.9 N (GPa)	AFM @ 90 µN (GPa)
	Through Ion Irradiated Surface	Cross Section Measurement
0	2.78 ± 0.04	5.0 ± 0.2
37	3.29 ± 0.03 (+18.3 %)	5.2 ± 0.1 (+4.0 %)
112	3.26 ± 0.05 (+17.3%)	5.5 ± 0.1 (+10.0 %)

2.5 Ion Irradiation Cross Sectional Analysis

SEM-EDS analysis was used to confirm the ion irradiated surface edge of the 112 DPA (i) sample by the presence of the 7.1 nm silver and 203 nm tungsten coating. Co-located AFM tapping mode analysis shows identical features, Figure 1Figure 10.

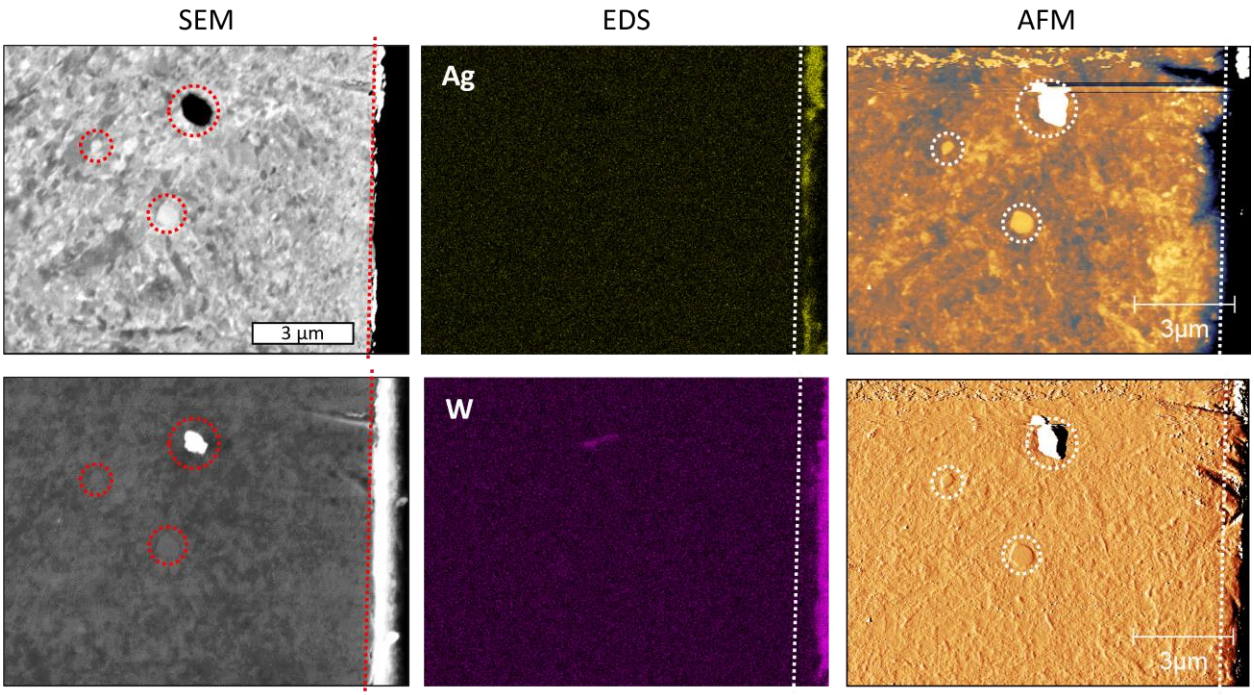

Figure 10. SEM and EDS analysis of the 112 DPA ion irradiated sample cross section revealing the silver/tungsten coating. Fiducial marks and the HT-9 edge are highlighted in the SEM and Co-located AFM.

Co-located AFM hardness mapping shown in Figure 11 (upper images) unfortunately failed during imaging and only a partial image was collected. No consistent and obvious delineation indicating the ion irradiated portion is observed, although a slight increase at the surface edge overall is apparent. The topographical image with hardness values overlaid (rightmost image) helps to interpret these results. The high values on the right side of the image show an erroneously high hardness value which is a tip artifact generated as the tip encounters the edge of the sample which changes the tip-sample interaction geometry. The 75 DPA (i) 37 DPA (n) ion irradiated surface edge does not show any indication of ion induced hardening.

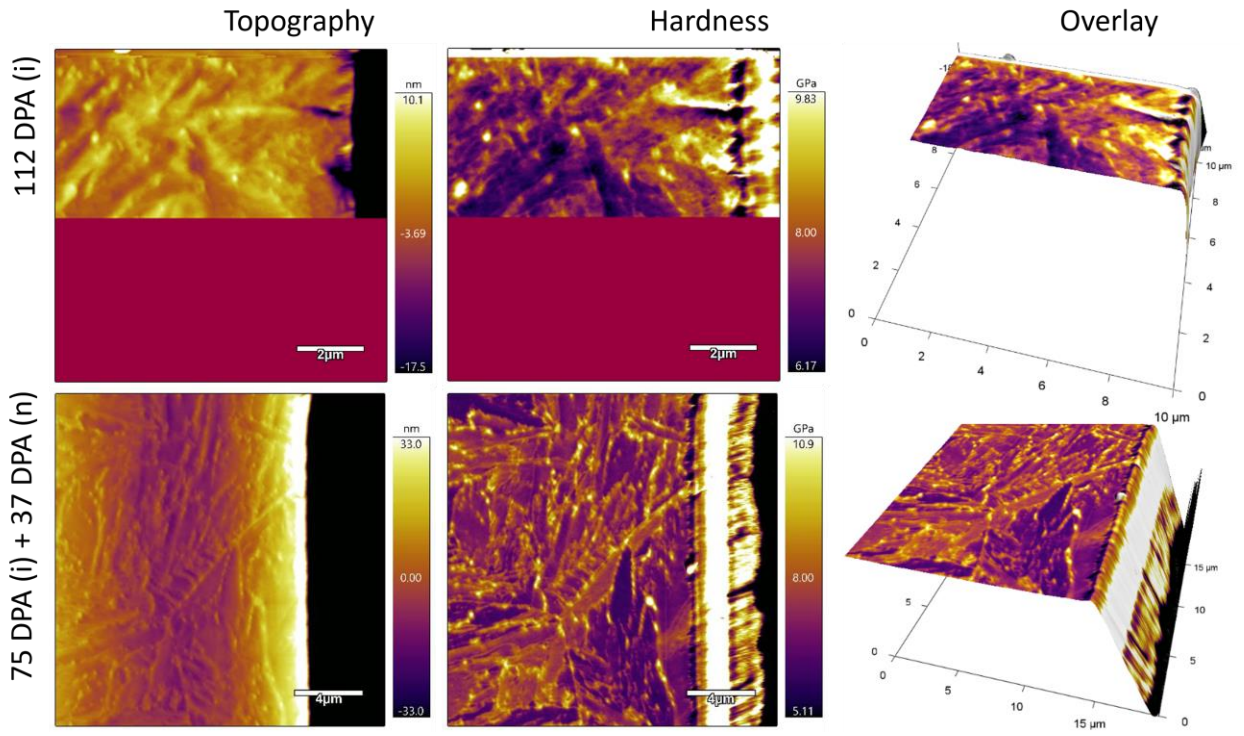

Figure 11. High resolution hardness mapping of the ion irradiated edge of the ion only and ion and neutron irradiated samples. The ion only image is co-located with the SEM and tapping mode AFM images in Figure 10. 3D topography / hardness overlays reveal the location of artificially high hardness values generated as a tip artifact at precipitous edges.

AFM hardness mapping of the opposite unprepared and unpolished surface edge reveals a region of increased hardness, Figure 12. This region is ~ 2 μm thick and shows a distinct difference in morphology for the 112 DPA (i) sample. For the 75 DPA (i) 37 DPA (n) sample this region is less distinct with a gradient ~ 8 μm thick. While this unpolished region is not the focus for understanding the HT-9 material it does provide an example of the resolution and ability to measure distinct hardness at the edge achievable by AFM hardness mapping.

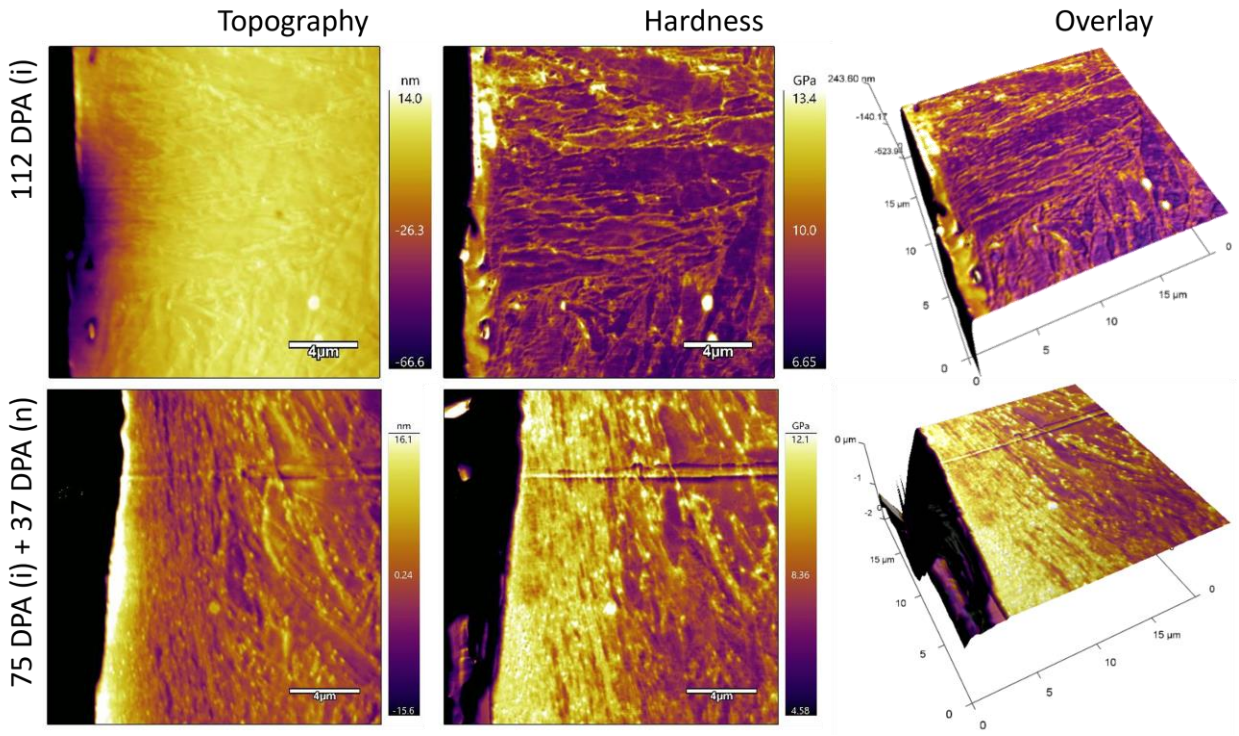

Figure 12. High resolution hardness mapping of the underside unpolished edge of the ion only and ion and neutron irradiated samples. Here the opposite artificially low hardness values off the edge are shown by 3D topography / hardness overlays.

Cursor profiles of the four surface edges better reveal hardness variation at the surface edges, Figure 13. The cursors are average over a width of 4 µm and show the hardness at the very edge relative to the topography and the precipitous drop where hardness values are no longer accurate.
Careful analysis of the 112 DPA ion irradiated surface edge reveals a thin region that may correspond to induced hardening of 0.53 GPa approximately 500 nm wide.

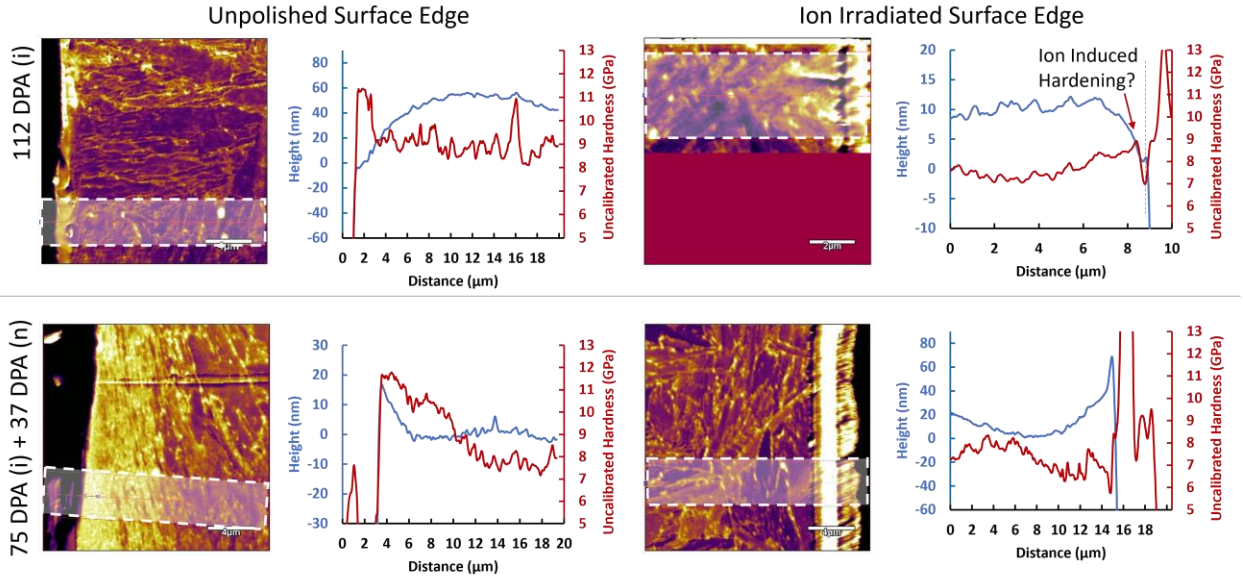

Figure 13. Cursor profiles at both the rough and polished / ion irradiated edges of the ion only and ion and neutron irradiated samples. Cursor plots are averaged across the regions highlighted in white shown on the hardness map images.

3.0 Summary

Legacy HT-9 samples provided a testbed for the analysis of neutron and ion irradiation by AFM hardness mapping. Optimized sample preparation including acetic acid treatment provided superior surface quality amenable to AFM analysis which is particularly sensitive to organic and particle contamination while not typically an issue for SEM. AFM hardness was optimized for newly acquired cube corner diamond probes to provide consistent high-resolution images with a lateral resolution down to ~150 nm. Calibration using NIST reference materials allowed for the comparison with previous microhardness analysis, where AFM hardness values were ~80% higher than reported Vickers hardness values. AFM hardness showed neutron hardening of 4% at 37 DPA (n) and 10% at 112 DPA (n). Analysis of the ion irradiated cross section did not show a consistent hardened region, but an averaged cursor did show an increase of 0.5 GPa at the outermost 500 nm, which may be a result of ion irradiation.

This work lays the foundation for further studies showing that AFM hardness is a feasible method for assessing fine local scale radiation hardening. Future endeavors should focus on a broader scope incorporating, for example, TEM analysis to assess ion irradiation to better validate the AFM hardness data. The higher ion irradiation dose legacy samples should also be analyzed as the larger penetration depth and void swelling will help to remove ambiguity and provide better confidence in the AFM analysis. In addition, AFM based scanning thermal microscopy, which was unavailable at the time of this work, should be employed. This technique provides analysis of the local thermal conductivity with higher resolution than is possible by AFM hardness mapping.

4.0 References

Kaspar, Tiffany C., Christina L. Arendt, Derek L. Neal, Shawn L. Riechers, Crystal Rutherford, Alan Schemer-Kohrn, Steven R. Spurgeon, Lucas E. Sweet, Vineet V. Joshi, Curt A. Lavender, and Rick W. Shimskey. 2019. "Characterization of surface layers formed on DU10Mo ingots after processing steps and high humidity exposure." *Journal of Nuclear Materials* 514:28-39. doi: https://doi.org/10.1016/j.jnucmat.2018.11.022.

Kautz, Elizabeth J., Miao Song, Shawn Riechers, Adam Koziol, Samuel A. Briggs, Kayla Yano, Ramprashad Prabhakaran, Alan Schemer-Kohrn, Ayoub Soulami, Vineet V. Joshi, and Arun Devaraj. 2023. "Influence of processing on secondary phase formation and microstructural evolution at U-10Mo alloy and Zr interlayer interfaces." *Journal of Alloys and Compounds* 969:172074. doi: https://doi.org/10.1016/j.jallcom.2023.172074.

Riechers, Shawn, and Brad Johnson. 2018. "Microstructural and Material Properties of Individual Zirconium Hydride Domains Formed Under Simulated Conditions." *Microscopy and Microanalysis* 24 (S1):1054-1055. doi: 10.1017/S1431927618005755.

Riechers, Shawn L., Andrew M. Casella, David J. Senor, and Pradeep Ramuhalli. 2020. "NSUF Rad-AFM: Nanoscale Material Property Measurements of Radioactive Materials." 122. doi: 10.13182/T122-32030

Journal Name: Transactions of the American Nuclear Society; Journal Volume: 122; Journal Issue: 1.

Riechers, Shawn L., Jesse B. Lang, Anthony D. Guzman, Brad R. Johnson, and Benjamin P. McCarthy. 2018. Material Properties of Zirconium Hydride Phases in Zircaloy-4 Getter Tubes Mapped by Atomic Force Microscopy. United States.

Pacific Northwest National Laboratory

902 Battelle Boulevard
P.O. Box 999
Richland, WA 99354

1-888-375-PNNL (7665)

www.pnnl.gov